

HIGH VELOCITY LINE EMISSION IN THE NLR OF NGC 4151¹

J.B. Hutchings

Dominion Astrophysical Observatory, National Research Council of Canada,
Victoria, B.C. V8X 4M6, Canada

D.M.Crenshaw², A.C.Danks³, T.R.Gull, S.B.Kraemer²

NASA's Goddard Space Flight Center, Lab for Astronomy and Solar Physics, Code 681,
Greenbelt MD 20771

C.H. Nelson, D. Weistrop

Dept of Physics, University of Nevada, Las Vegas, 4505 Maryland Pkwy, Las Vegas, NV
89154-4002

M.E.Kaiser

Dept of Physics and Astronomy, Johns Hopkins University, Baltimore, MD 21218

C.L.Joseph

Dept of Physics and astronomy, Rutgers University, Piscataway, NJ 08855-0849

ABSTRACT

Narrow-band imaging of the nuclear region of NGC 4151 with the Hubble Space Telescope is presented. The filter bandpasses isolate line emission in various high velocity ranges in several ions. Slitless and long-slit spectra of the region with the Space Telescope Imaging Spectrograph also indicate the locations of high velocity gas. These emission regions are faint and are interspersed among the bright emission clouds seen in direct images. They have radial velocities up to 1400 km s^{-1} relative to the nucleus, and are found in both approach and recession on both sides of the nucleus. This contrasts strongly with the bright emission line clouds which have been discussed previously as showing bidirectional outflow with velocities within 400 km s^{-1} of the nucleus. We discuss the possible connections of the high velocity material with the radio jet and the nuclear radiation.

¹Based on observations with the NASA/ESA *Hubble Space Telescope*, obtained at the Space Telescope Science Institute, which is operated by AURA Inc under NASA contract NAS5-26555

²Dept of Physics, Catholic University of America, Washington DC 20064

³Raytheon ITSS

Subject headings: galaxies: Seyfert, galaxies: individual (NGC 4151), line: formation

1. Introduction

The Seyfert galaxy NGC 4151 is close enough and well oriented to enable a detailed study of the associated cloud structure around the nuclear engine, with the ultimate goal of understanding the Seyfert mechanism. HST instrumentation has advanced these studies with its high spatial imaging (e.g. Evans *et al* 1993, Boksenberg *et al* 1995, Winge *et al* 1997). The power of HST was greatly extended by the installation of the Space Telescope Imaging Spectrograph (STIS), with both slitless and longslit capability. The structure and kinematics of the narrow line region of NGC 4151 have been studied recently using slitless spectra obtained with STIS (Hutchings *et al* , 1998, Kaiser *et al* , 1999). More detailed investigation along subsequently defined long slit locations have been done by Nelson *et al* (1999) and Kraemer *et al* (1999). This work revealed a much fuller picture of the kinematics and ionization structure of the ensemble of emission line clouds that form a "biconical" region on both sides of the nucleus and roughly along the axis of the extended radio structure on either side of the nucleus. The majority of the clouds appear to be outflowing from the nucleus at velocities $<400\text{km. s}^{-1}$, approaching us to the west side and receding on the eastern side. These clouds appear to be part of a general outflow away from the nucleus, but they are not obviously connected with the radio jet outflow. Beyond the inner 5 arcsec, the emission line clouds have lower velocities and appear to be participating in the general galaxy rotation rather than under any influence of the nuclear processes. They do appear to be illuminated and ionized by the beamed nuclear radiation.

In the course of the work on the bright clouds, some weaker and highly shifted emission components were seen in the slitless spectra. Kaiser *et al* (1999) identified 6 of these with velocities ranging from +846 to -1716 km s $^{-1}$. The location of the material with these high velocities was established by use of two different dispersion directions in the slitless data, as described by Kaiser *et al* . These locations did not generally correspond with any bright region seen in the undispersed narrow band images, but lay within the ensemble of such clouds, which have much larger flux than the high velocity material, as measured from the dispersed images.

The high velocity material did not fit the simple biconical outflow scenario that describes the bright clouds, and Kaiser *et al* noted that there seem to be more than one

kinematic components superposed in the region. In addition, there is a bimodal distribution of velocity dispersions among the bright clouds that is not related to the radial velocity, although the high velocity clouds all have high velocity dispersion.

In order to study the high velocity material in more detail, and to distinguish it from the bright clouds, we obtained a number of narrow band filter images with STIS and WFPC2. These have bandpasses near to the wavelengths of several strong emission lines, and comparison between them was intended to indicate the location of emission material in various velocity ranges. In all cases, these ranges are more than 400 km s^{-1} from that of the nucleus, and thus help isolate the high velocity gas.

We report here on these imaging data, and use them in conjunction with the slitless spectra, and two long-slit STIS spectra through the region, to discuss the high velocity gas in the nuclear region of NGC 4151.

2. Image data

Table 1 shows the observational log. The redshift of NGC 4151 is close to 1000 km s^{-1} , and the high velocities range over more than 2000 km s^{-1} about that, so that the bandpasses of the narrow-band filters do not in general include all the velocities present in the region. Figure 1 illustrates the velocity ranges that are covered for the lines in the passbands, as defined by the FWHM of their transmission functions. In several cases there are two or more lines within the passband, so that different velocities are sampled for the different lines. These are the [O II] 3727A doublet and the [S II] 6717-31A doublet, and the [N II] plus H α triplet at ~ 6548 -84A. We also obtained continuum images and used an archival F502N image from WFPC2.

Figure 2 shows some images and differences of interest. The LRF image of [O III] covers all known velocities from the slitless data, and thus is the full representation of the [O III] flux. The STIS [O III] image covers velocities between -1200 and -860 km s^{-1} with respect to the nucleus. It shows almost no resemblance to the LRF image, and some of the bright knots are in areas of low flux in the total intensity image. Thus, the high velocity material in this velocity range is much fainter than the main bright clouds. It also is seen on both sides of the nucleus and outside the main biconical emission region. The difference between the F502N and LRF image shows regions of high positive velocity. These too do not correspond with the main bright knots, and lie on the E side of the nucleus.

The other difference images in Figure 2 are more complex as they compare different lines and combinations of lines. They do however indicate the same regions of high positive

and negative velocity, although the contrast is lower because of including continuum or some flux from the low velocity lines.

3. Spectroscopic data

The slitless spectra have been described fully in the Hutchings *et al* and Kaiser *et al* references. In Figure 3 we show one of the [O III] 5007A line, intended to show the high velocity material clearly. The locations of the high velocity material in the total [O III] image are shown in Figure 4. The long slit data are described in detail by Nelson *et al* (1999). For the purpose of this paper we show the orientation of the two 0.1" wide slits in Figure 5.

From the slitless data we can locate the high velocity regions labelled with letters in Figures 4 and 5. These positions depend on identifying the same feature in both dispersed images. In crowded regions there is occasionally some ambiguity between regions that lie along the same dispersion direction. The image data have been valuable in showing up regions where some high velocity material lies, and provide significant overlap with the slitless spectra.

The two long slit spectra do not sample the whole region, but they do reveal a few high velocity regions that correspond with (parts of) H, D, N(=26), and M, as well as verifying the bright knot velocities reported in the slitless papers (see Figure 5). Table 2 shows the velocities from all our spectroscopic data. These differ from values given for some of them by Kaiser *et al* (1999), mainly because of more detailed attention to these weak features. The differences are in most cases within the uncertainties, and in most cases the large line width (often blended with other stronger features) make the values reliable only within $\sim 10\%$ of their given value.

The long slit data do not show any signs of E, F, B, C, I, or J, although their estimated positions lie close to the slits. The positions for H and D also lie near the slit edges, but so do G and A, which have similar velocities. It is thus possible that there is extended high velocity emission lying between G-H and A-D. Since there is no doubt of the reality of the high velocity material at E, F, B, C, I, and J in the slitless images, we conclude that either the regions are compact, or faintness and uncertainty in their locations explains why they are not seen in the long slit data.

The long slit data do indicate material with high positive velocity ($+400 \text{ km s}^{-1}$) near bright cloud 19 of Hutchings et al (1998), and some material at $\sim -600 \text{ km s}^{-1}$ inside region M. The STIS [O III] image also indicates regions of high negative velocity marked

with small squares in Figure 4. These are not seen in the slitless data as these velocity shifts place the dispersed line emission in the region dominated by the bright emission clouds. Thus, it is clear that we do not have the complete picture of high velocity emissions, and that a full set of long slit spectra, possibly with different orientations, would be required to get that.

However, with the exception of bright knot 26, the high velocity line emission has low flux and comes from locations superposed on the whole inner bright emission cloud region. Region O also lies at the end of a plume of material seen extending out of the main emission cloud region, although very close to the nucleus.

Winge *et al* (1999) report velocities from several long slit spectra obtained with the FOC. These have lower resolution and S/N and greater distortions than the STIS spectra. However, their results also show up high velocity material that stands apart from the lower velocities found in the main cloud ensemble. Their results detect the material we designate N and G-H in their nuclear spectrum; C and G-H in their 0.23" NW offset; D and the knots seen in the STIS [O III] image in their 0.41" and 0.46" offsets to the NW. Thus their results are consistent with those reported here.

4. Ionisation structure

With the complete wavelength coverage of the [O II], [O III], and H β line velocities in our images, it is possible to construct ratio images that show the variation of O ionisation and [O III]/H β in the emission line region. Figure 6 shows these ratios. The [O III]/[O II] ratio was not corrected for the different continuum and nuclear scattering in the two images, but these appear to be small as there is no systematic gradient away from the nucleus. Both ratio images were tested empirically for sensitivity to alignment, sampling, and rotation and the morphological features that are seen are robust to any expected uncertainties.

We first note that the ionisation of O is higher along radial locations on both sides of the nucleus. The rays are longer to the W, which is the approaching side for the general outflow. This suggests these are paths where the nuclear radiation is less obscured, and ionise the gas more strongly. These paths are seen more clearly in the approaching cone. Making a detailed comparison with the high velocity gas locations, we find that many of them lie in the regions of higher ionisation. Some (e.g. G and H, B, C, I, J lie around the edges of a high ionisation region. A few (E, F, and A) lie in regions of low or average ionisation. Region O lies in the part of the diagram affected by the telescope diffraction spikes, so we cannot comment on it. Generally there is an association of high velocity with

higher ionisation. There are, however regions of high ionisation (mainly to the E) with no known high velocity gas. In view of the higher signal from the bright clouds and the fact that not all high velocity regions appear to lie in high ionisation places, we need to confirm these conclusions with systematic slit spectroscopy.

Turning to the $[\text{O III}]/\text{H}\beta$ ratio, there is good signal over a smaller region, but the main radial features are still present. This presumably is a result of the same cause: where O is more highly ionised, the H is weaker because it is ionised. Kaiser *et al* have discussed the quantitative $[\text{O III}]/\text{H}\beta$ values for many bright clouds based on dispersed images. The present images will superpose the high velocity fluxes on the bright clouds, and the latter presumably dominate. In detail, the high velocity gas locations lie in or close to regions of high $[\text{O III}]/\text{H}\beta$, even more markedly than the O line ratio. Once again, we have a few regions of high ratio that do not lie near any known high velocity gas, and the same cannot apply to any general conclusions about the high velocity gas.

Thus, the high velocity gas is weak in $\text{H}\beta$ and $[\text{O II}]$, and appears to occur in highly ionised material. In the bright clouds Kaiser *et al* find a decrease in $[\text{O III}]/\text{H}\beta$ with increasing nuclear distance. The high velocity gas has higher $[\text{O III}]/\text{H}\beta$: it is not known how high but the non-detection in $[\text{O II}]$ and $\text{H}\beta$ implies numbers larger than 15. The measured bright cloud line ratios from Kaiser *et al* do not show up as features in the ratio image, so that there may be gradients within large clouds, or confusion from overlap. Table 2 shows nuclear distances for the high velocity regions, and there is no correlation of line ratio with this: the regions all lie within the high ionisation inner region of Figure 5.

5. Radio structure

The radio structure of NGC4151 lies along a line with the brightest feature at the nucleus. There are several bright knots along the structure, on both sides of the nucleus, but with more flux and structure on the E (approaching) side. As noted in Kaiser *et al* , there is little detailed correspondence between the bright clouds and the radio structure, although the radio axis lies along the overall inner emission line region. In addition, the innermost radio structure shows a bend away from the large-scale axis by some 50° (to the N), but on a spatial scale unresolved by HST.

Figure 4 shows the radio structure ridge line and the locations of the main bright features at 6cm. The brightest knot C3 lies close to the brightest emission line cloud #20 from Hutchings *et al* . Several high velocity gas locations lie close to the radio ridge line (E, F, D, A), while others occur near bright radio knots or bends in the ridge line (G, C,

I). About half the high velocity locations do not have any apparent relationship to the radio structure. There is no correlation between the magnitude of the gas velocity and the projected distance from the radio jet. There is also no high velocity material in the direction of the innermost (VLBI) radio jet orientation.

6. Discussion

Table 2 summarizes what is known about the high velocity material. The high velocity gas appears to be a different kinematic component of the nuclear environment from the bright biconical clouds. The high velocity gas has higher ionisation, probably due to less obscured illumination by the nucleus. The material has much lower flux (by more than an order of magnitude in [O III] flux, and even more in other lines) than the bright clouds, with the single exception of cloud 26 whose flux is typical of the bright clouds. The high velocity material is seen with velocities of approach and recession on both sides of the nucleus, quite distinct from the clear separation of approach and recession across the nucleus, in the bright clouds.

The location of the known high velocity material (which is probably not complete) is along ridges of higher ionisation. The ridges are more marked and longer on the W side, where the bright clouds are approaching (i.e. the near side of the bicone). The central ridge lies along the line of the radio jet axis, and the radio ridge line appears to wind around regions of highest ionisation (Figure 4). This may indicate that the jet is deflected by higher density in these regions, or that it adds to the ionisation by its interaction with gas clouds, as proposed in a more general sense by Winge et al (1999).

12 of the 17 known regions of high velocity material lie in the W (approaching) cone. This implies that there is less overall obscuration on this side, considering that the flux from all such regions is low. There is no flux difference across the nucleus, in the regions that are seen. The high velocity material does appear to be distinct from the bicone outflow inferred from the bright clouds, but its overall velocity and visibility is consistent with that picture.

All of the high velocity material has a high velocity dispersion, by the criterion of 130 km s^{-1} set by Kaiser *et al*. Some of the velocity dispersions (as noted in the table) are much higher, but also not well determined because of blending in the slitless images. However, there are also high velocity dispersion bright clouds with low radial velocities, as shown by Kaiser *et al*. There are some 10 bright clouds that have velocity dispersions comparable with the low flux high velocity regions. High velocity gas is found only within about 1 arcsec of the nucleus, and all high velocity dispersion material lies within about 2

arcsec of the nucleus.

It is tempting to suppose that the high velocity material is accelerated radially away from the nucleus with a velocity gradient that is also radial. That would predict that there is a correlation between radial velocity and velocity dispersion due to projection effects, and we do not in fact see clear evidence of this. Also, it would not explain why there are bright low velocity, high velocity dispersion clouds. Thus, it appears that this effect is not a strong one, and high velocity dispersion is found in both populations - bright outflow clouds and the high velocity gas.

The high velocity gas is generally lower in density and appears in places that may be directly illuminated by nuclear radiation or shocked by nuclear material. The coincidence with radio features may indicate that the jet also moves along one line of direct illumination (travel) from the nucleus, rather than direct acceleration of the high velocity gas by the jet.

The fact that velocities of approach and recession are not connected with position E or W of the nucleus suggests that the whatever drives the high velocity material may push it aside from the general radial motion, so that it may appear with radial velocity counter to the general flow, by projection. It may be that there is high velocity material projected with low radial velocity that is not recognised against the backdrop of lower velocity motions of the bright clouds. We also note that the high velocity material may be consistent with the ballistic ejection model proposed by Smith (1994), as it is faint, has large velocity dispersion, and may be highly ionised.

Finally, we note that the high velocities are similar to those seen strongly in absorption in C IV, against the nucleus. However, those absorbers have very low velocity dispersions (Weymann *et al* 1997), with one exception. The exception is a broad transient absorber seen at high approach velocity in one GHRS spectrum. The location of the high velocity emitting gas suggests a low covering factor against the nucleus from our line of sight. The relationship of the narrow high velocity C IV absorbers to the optical high velocity emitters is not clear.

References

Boksenberg A., *et al* , 1995, ApJ, 440, 151

Evans I.N., Tsvetanov Z., Kriss G.A., Ford H.C., Caganoff S., Koratkar A.P., ApJ, 417, 82

Hutchings J.B., *et al* 1998, ApJ, 492, L115, 1998

Kaiser M.E., *et al* 1999, ApJ (in press: astro-ph 9906283)

Kraemer S.B., Crenshaw D.M., Hutchings J.B., Gull T.R., Kaiser M.E., Nelson C.H., Weistrop D., 1999, preprint

Nelson C.H., Weistrop D., Hutchings J.B., Crenshaw D.M., Gull T.R., Kaiser M.E., Kraemer S.B., Lindler D., 1999, preprint

Pedlar A., *et al* , 1993, MNRAS, 263, 471

Smith M.D., 1994, MNRAS, 209, 913

Weymann R.J., Morris S.L., Gray M.E., Hutchings J.B., 1997, ApJ, 483, 717

Winge C., Axon D.J., Macchetto F.D., Capetti A., 1997, ApJ, 487, L121

Winge C., Axon D.J., Macchetto F.D., Capetti A., Marconi A., 1999, astro-ph 9901415

Captions to Figures

1. Ranges of radial velocity with respect to NGC 4151 nucleus covered by narrow-band filters, for emission lines that lie within their passbands. The filters are shown and exposures are listed in Table 1. The dots in the bottom row indicate the approximate velocities of the known high velocity emission lines in NGC 4151. The range between -400 and 400 is occupied by almost all the bright emission line clouds.
2. Images and difference images of the central ~ 5 arcsec of NGC 4151, as labelled. The orientation is the same for all and North is indicated in Figure 4. The central emission line region shown is approximately 1×4 arcsec. The bright clouds are approaching on the lower side and receding on the upper side of the nucleus. The material visible has velocity ranges as shown in Figure 1. Individual images are discussed in the text.
3. A slitless spectral image of [O III] line showing dispersed locations of high velocity material. The lower panel is the unprocessed image with the nuclear continuum removed, and stretch to show the faint high velocity components. The upper panel is an unsharp mask that shows some of the high velocity features more clearly.
4. Positions of high velocity material identified on the total [O III] image. Table 2 gives details of the individual positions as labelled. The key shows how the positions are derived. The jagged line sketches the ridge of the radio structure, with its bright knots identified by X and numbered following Pedlar *et al* 1993. The arrow indicates North.
5. The positions of our long slits shown with respect to the lettered high velocity material from Figure 3. The slit widths are somewhat oversized and relative positions of the high velocity gas are uncertain by up to $0.1''$.
6. Matched [O III] and ratio images of central NGC 4151. Note the radially extended regions of higher ionisation, particularly to the W (lower right). The images are discussed in the text.

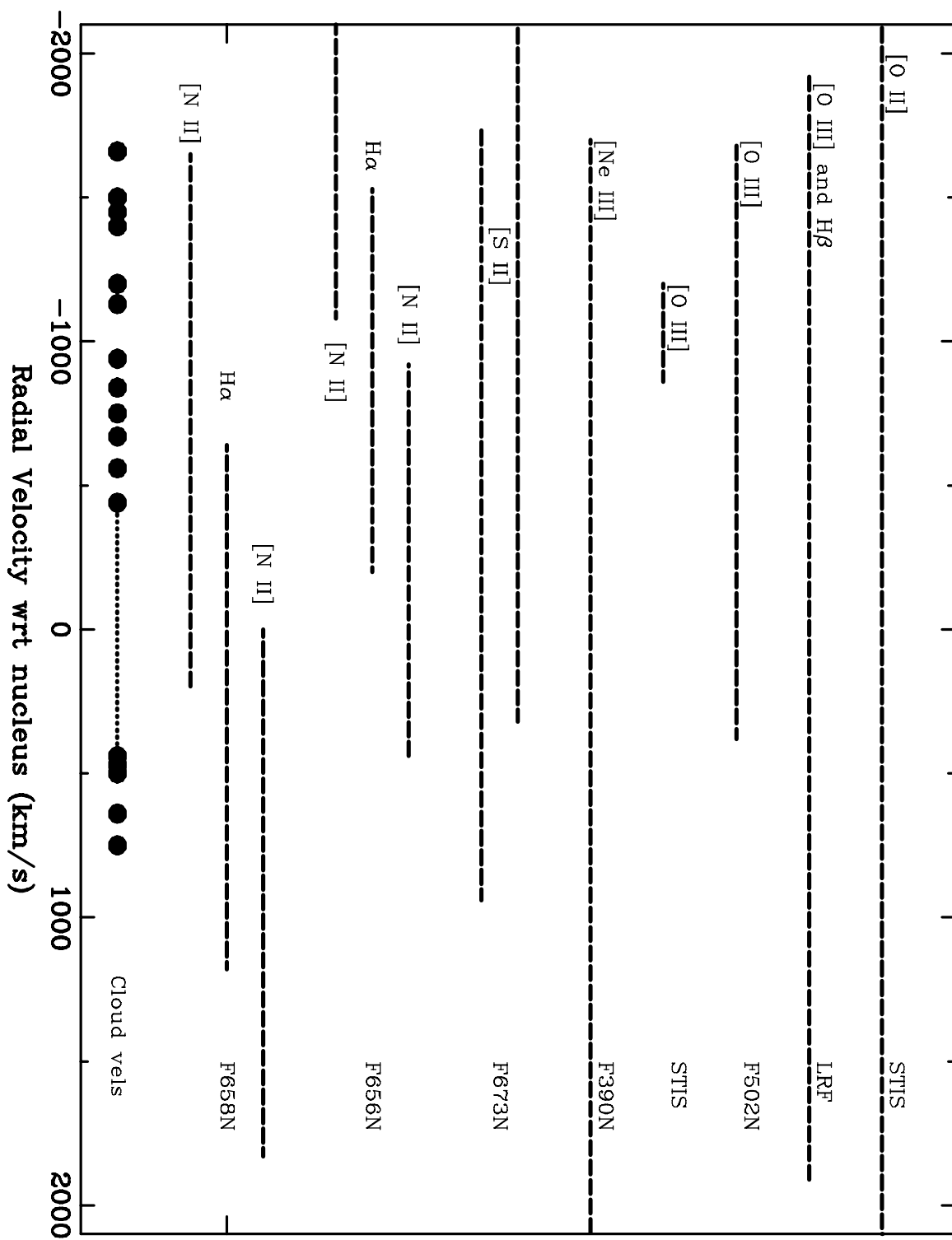
Table 1. NGC 4151 Journal of observations

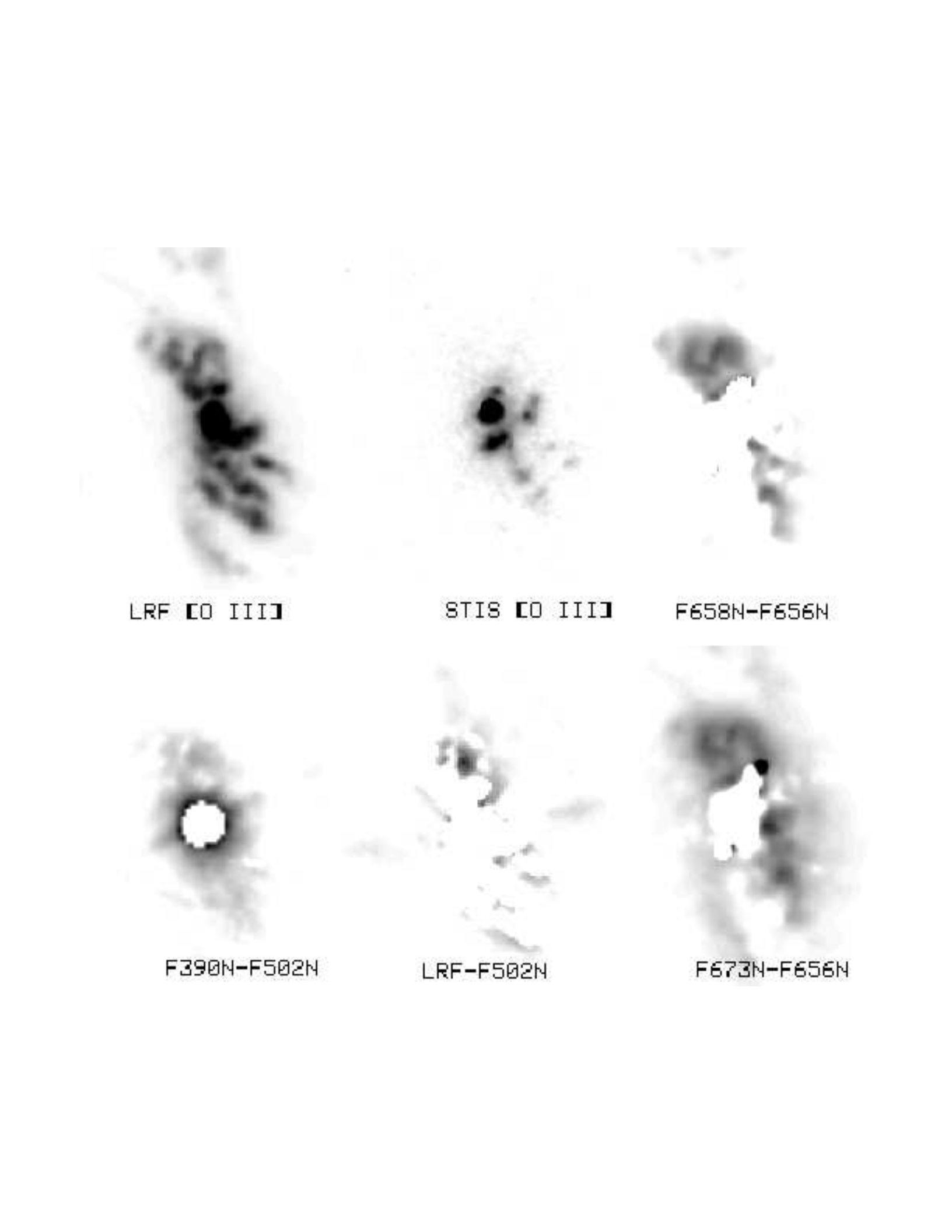
Instrument	Filter	Exp (sec)	Date	Dataset
STIS	[O II]	300	Dec 1996	o3vs01030
	[O III]	300		o3vs01040
WFPC2	F502N	870	Jan 1995	v2i50101A
	F658N	402	Apr 1998	u4230601A
	F390N	1200		u4230604A
	F673N	1200		u4230606A
	F656N	700		u4230608A
	F547M	10	Feb 1999	u5780207-8R
	FR533N [O III]	140		u5780203-4R
	FR533N H β	300		u5780205-6R

Table 2. NGC 4151 high velocity emission lines

Region	RV ^a km s ⁻¹	Nuclear distance	Radio ridge distance	Ionisation	Notes
A	-1450	1.7"	0"	Average	
B	-1300	1.6"	0.3"	Average	
C	-900	1.5"	0.15"	High	
D	-1200	1.5"	0"	Peak	In long slit
D'	400	1.6"	0.1"	Average	Longslit only, at cloud 19
E	-380	1.8"	<0.1"	High H?	Max RV -500
F	-440	2.0"	0"	High H?	
F'	-290	2.0"	-	-	Co-located with F
G	730	1.5"	0.15"	Peak	Max RV 990, Near radio C5
H	650	1.6"	0.2"	High H?	Max RV 820
I	700	1.7"	0.1"	High	Near radio bend
J	650	1.7"	0.3"	Average	
M	-1150	0.4"	0.15"	High	Close to nucleus
N=26	-760	0.6"	0.15"	High	Bright cloud 26
O	-870	1.0"	0.5"	High?	Normal to jet, in STIS image
STIS	^b	0.8"	0.2"	Peak	Only in STIS image
STIS	^b	1.5"	0.2"	Peak	Only in STIS image
STIS	^b	2.0"	0.4"	Peak	Only in STIS image

^aWith respect to nucleus^b-860 to -1200





LRF [O III]

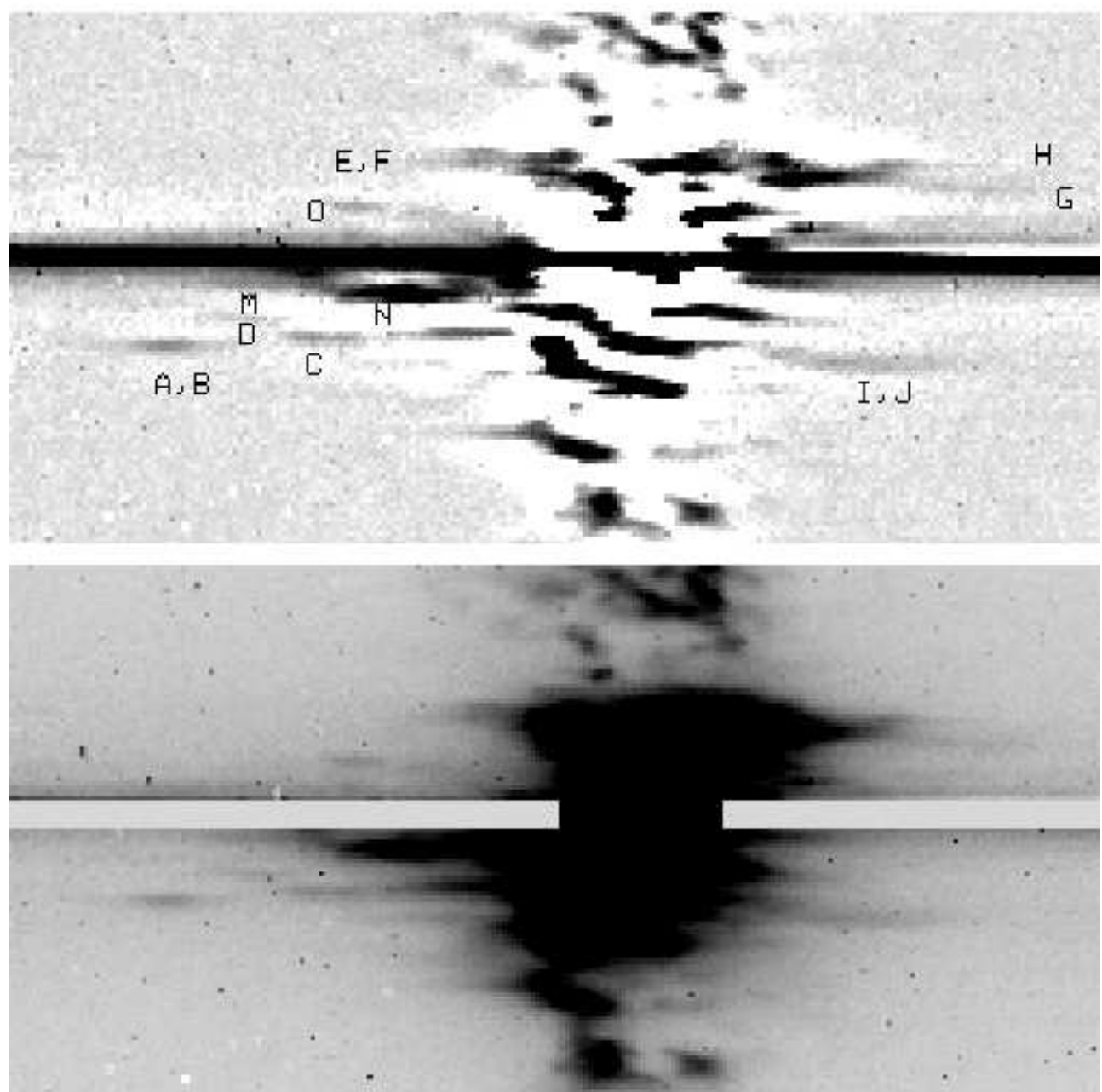
STIS [O III]

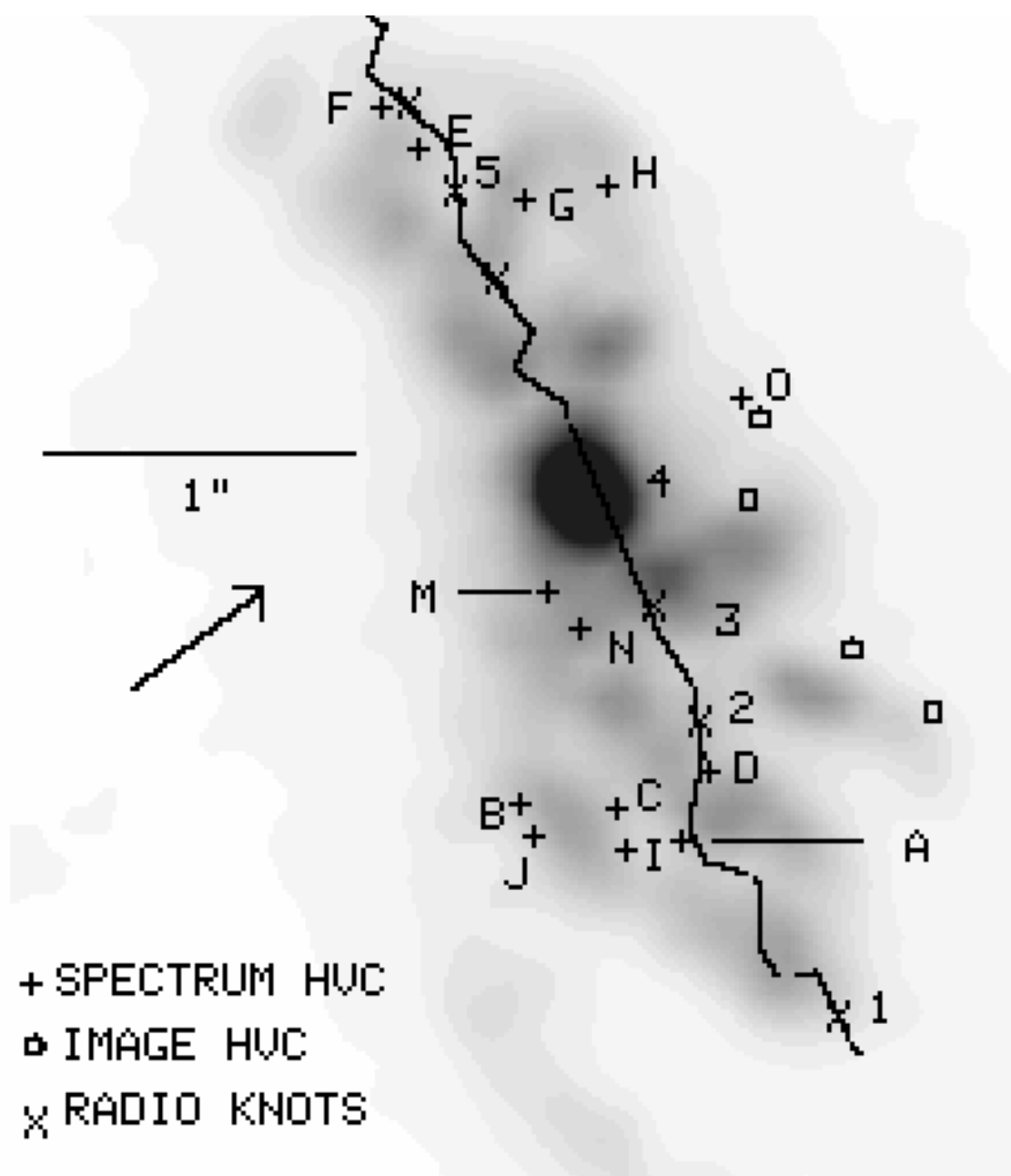
F658N-F656N

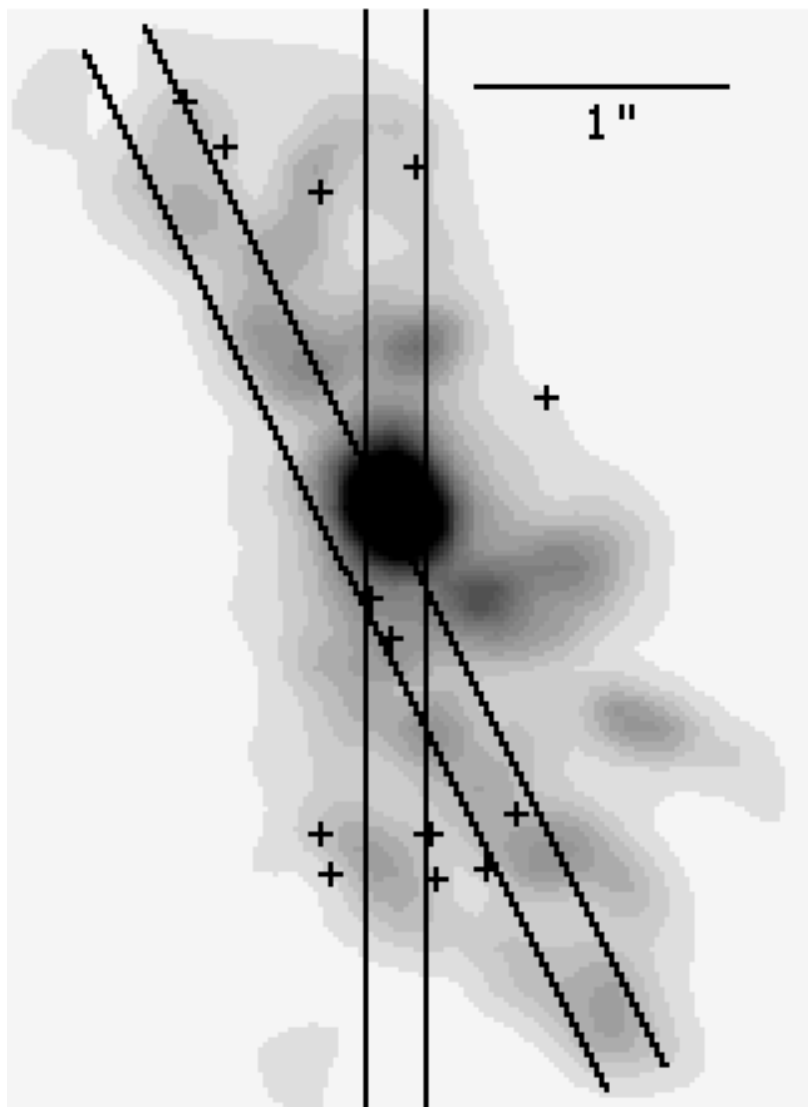
F390N-F502N

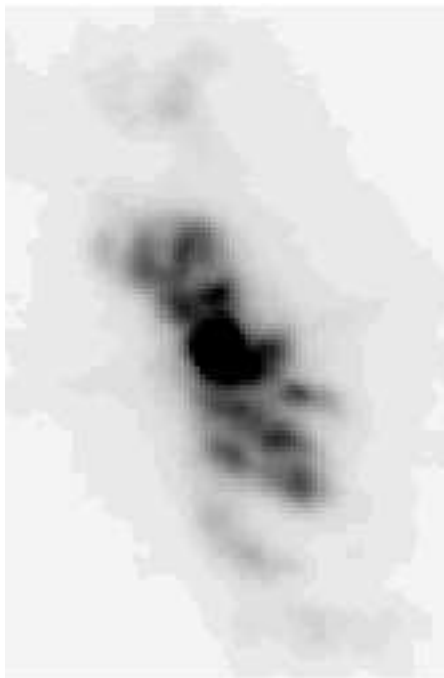
LRF-F502N

F673N-F656N

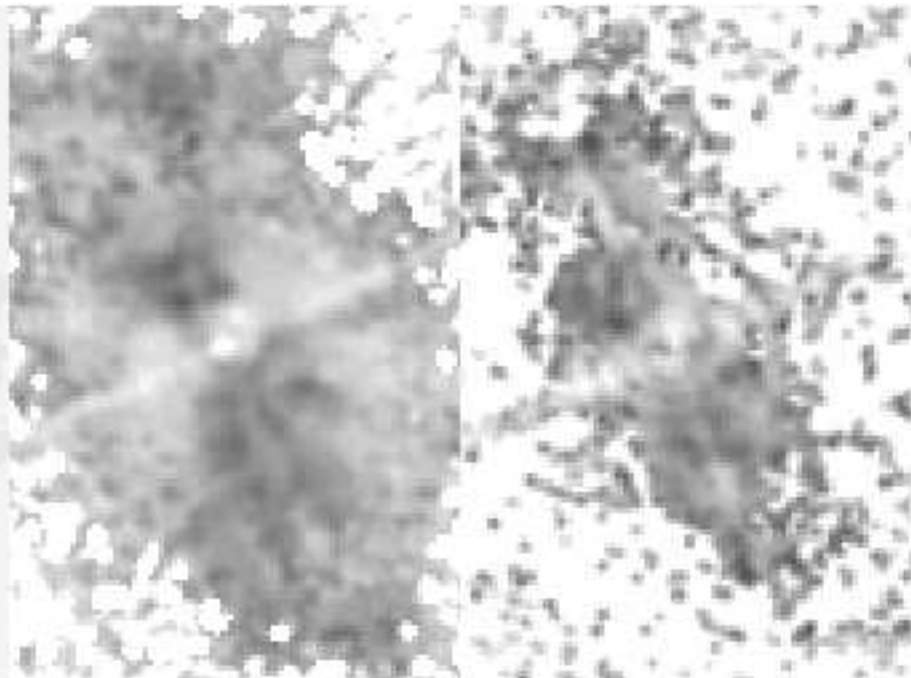








O III



O III/ O II

O III/ H